Rotating Ring Disk Electrode for Monitoring the Oxygen Release at High Potentials in Li-Rich Layered Oxides

Wei Yin, Sathiya Mariyappan, Alexis Grimaud, J.-M. Tarascon

Rotating Ring Disk Electrode for Monitoring the Oxygen Release at High Potentials in Li-rich Layered Oxides

Wei Yin, [†, ‡] Sathiya Mariyappan, [† ‖] Alexis Grimaud[†, §]*and J.M. Tarascon [†, §, ‖, ‡]

[†]Chimie du Solide et de l'Energie, UMR 8260, Collège de France, 75231, Paris Cedex 05, France

[‡]Sorbonne Université - UPMC Université Paris 06, 4 place Jussieu F-75005 Paris, France

[§]Réseau sur le Stockage Electrochimique de l'Energie (RS2E), CNRS FR 3459, 33 rue Saint Leu, 80039, Amiens Cedex, France

[‖]ALISTORE-European Research Institute, FR CNRS 3104, 80039 Amiens, France

*Corresponding author: Alexis Grimaud <alexis.grimaud@college-de-france.fr>

Abstract

Li-rich layered oxides show a staggering capacity that relies on cumulative cationic and anionic redox processes. However, their practical applications are plagued by roadblocks dealing with large hysteresis, capacity fade and irreversible oxygen loss during the first charge that causes undesirable structural changes. Hence, the first step to screen the Li-rich layered oxides is the identification of this gas release phenomenon and its better understanding. Differential electrochemical mass spectrometry (DEMS) is presently used for the elucidation of gas evolution, but its usage is lengthy and far to be routine. Herein we propose the utilization of the simple rotating ring disc electrode (RRDE) technique for the identification of O_2 release phenomenon and hence the quick screening of Li-rich layered

oxides. We have evaluated the feasibility of RRDE to monitor the O_2 generation by conducting studies on Li-half cells having various Li-rich layered oxides as cathodes and found that our results nicely compare with those obtained by DEMS, hence demonstrating the validity of RRDE technique. The proposed RRDE approach which offers high sensitivity for the identification of O_2 release while being fast and simple should greatly help to advance the understanding of oxygen redox processes and promote the design of new materials.

Introduction

After making its mark in portable electronics, the lithium-ion battery technology is now gaining increasing importance for applications such as electric vehicles and grid storage. To meet the ever-growing demand for improving continuously the energy-density of this technology, extensive research efforts have been directed toward the development of positive electrodes with higher redox voltages and/or greater capacities. Within this framework, the recent discovery of the lattice oxygen redox activity has effectively unlocked the capacity limitation of positive electrodes which was previously believed to be pinned by the redox activity of transition metals.[1-3] Even though the combination of cationic (transition metal) and anionic (oxygen) redox activity can enhance the capacity well beyond what the sole cationic redox can offer with capacities exceeding 280 mAh g^{-1} for $Li_{1.2}Ni_{0.13}Mn_{0.54}Co_{0.13}O_2$ as compared to solely 180 mAh g^{-1} for $LiNi_{1/3}Mn_{1/3}Co_{1/3}O_2$,[4, 5] several issues such as voltage decay, sluggish kinetics, hysteresis, first cycle irreversibility, etc. still remain to be addressed prior to envision any practical application for these Li-rich layered compounds.[6, 7] To circumvent these issues, the mechanism of oxygen redox reactions in

these oxides has to be understood. Most of the Li-rich layered oxides studied so far exhibited O_2 release phenomenon on charge, the extent of which depends on the nature of the material and the oxidation potential.[8-10] Combined experimental and theoretical calculations have shown that such O_2 release which affects the materials' performances (capacity fading, ...) is unfortunately the largest for the 3*d* metals which present the greatest interest practical-wise. [3, 11-14]

A straightforward approach to probe the irreversible oxygen loss phenomenon is to employ *in-situ* gas/pressure analytical techniques which can directly analyze the gaseous products formed upon battery operation. Currently, two of such techniques have been heavily implemented. The first one is the differential (or online) electrochemical mass spectrometry, also termed DEMS (or OEMS). It couples an electrochemical cell with both a vacuum system and a quadrupole mass spectrometer which analyzes the gases sampled in the head space of the cell.[8, 9] This technique allows for the identification and the quantification of various gaseous species, and thus has helped to advance the understanding of complex electrochemical processes for Li-rich materials and to promote their rational design and optimization.[9, 15] Nevertheless, the disadvantages related to the use of OEMS are nested in the complexity of such technique, as wells as its high cost and sensitive operation, which currently hampers its day-to-day use for screening series of materials. Such limitations have led to the development of another technique termed pressure cell and which simply integrates a pressure sensor to a laboratory Swagelok-type cell, which thus can be easily implemented and enable long-time gas monitoring.[16-18] However, the main drawback of this rather user-friendly approach relies on the fact that it only measures the pressure change, and thus does not allow for determining the nature of the gases evolved upon operation.

These limitations were a motivation to search for a more user-friendly and accurate technique to rapidly screen new materials with respect to their electrochemical stability against O_2 release.

Developed about fifty years ago, the rotating ring disk electrode (RRDE) technique has proven to be a powerful tool for investigating short-lived intermediate species generated in electrochemical reactions.[19, 20] Benefiting from the laminar electrolyte flow created by the mechanical rotation and the existence of double concentric working electrodes (disk and ring electrodes) separated by a non-conductive barrier, products generated at the disk electrode are swept across the surrounding ring electrode along with the electrolyte flow, allowing for their electrochemical detection at the ring.[19, 20] Therefore, RRDE has been widely applied to study the reaction kinetics and transport properties for the oxygen reduction reaction (ORR) relevant to metal-air batteries and proton exchange membrane (PEM) fuel cell,[21-27] as well as to probe intermediates of lithium-sulfur redox reactions,[28] to study the manganese dissolution of spinel-based cathodes,[29] to survey the dissolution of metal ions during the corrosion processes,[30, 31] and to determine the faradaic efficiency of oxygen evolution reaction (OER) electrocatalysts for water splitting, [32, 33] among other usages.

In this work, we introduced RRDE as a sensitive *operando* method for monitoring the O_2 evolution during cycling of Li-rich layered oxides at high potentials. For that purpose, the oxides of interest are deposited onto the surface of the disk electrode and then cycled in classical linear scan voltammetry, cyclic voltammetry and/or galvanostatic mode. Simultaneously, the O_2 release phenomenon is assessed by collecting (reducing) at the ring electrode the generated gaseous oxygen. Two families of layered oxides (Li-stoichiometric

and Li-rich NMCs as well as $Li_2Ru_{1-y}Ti_yO_3$ phases) were chosen for initial evaluation. Furthermore, a comparative study of the proposed RRDE method with the existing pressure/gas analysis techniques such as pressure cell and OEMS was carried out. We expect this approach to be beneficial in evaluating the nature of the oxygen redox reactions for high-capacity cathode materials involving cumulative cationic and anionic redox chemistry.

Experimental

Materials.—$Li_{1.2}Ni_{0.13}Mn_{0.54}Co_{0.13}O_2$ was prepared by coprecipitation combined with solid-state synthesis,[5] $Li_2Ru_{0.75}Ti_{0.25}O_3$ and $Li_2Ru_{0.5}Ti_{0.5}O_3$ were prepared by classical solid-state synthesis, as described in details elsewhere.[34] $LiNi_{1/3}Mn_{1/3}Co_{1/3}O_2$ (>98%) and carbon super P were purchased from Sigma-Aldrich and MTI Corporation, respectively. LP30 electrolyte (99.9%) made of 1 M $LiPF_6$ dissolved in 1:1 v/v Ethylene carbonate/Dimethyl carbonate was purchased from Solvionic, France.

RRDE setup.—Fig. 1 shows the schematic illustration of the RRDE system with a four-electrode cell configuration. All the experiments were performed in an argon filled glovebox (water content < 0.5 ppm, oxygen content < 0.1 ppm) with a five-neck glass cell sealed with rubber stoppers, except a bubbler which was connected to a gas line that allows feeding the cell with dry argon (5.0 quality, Linde France), and a needle which was inserted into the cell as a gas outlet. The RRDE tip consists of an inter-changeable glassy carbon disc of 5.0 mm in diameter and a platinum ring with an internal diameter of 6.5mm and an external diameter of 7.5 mm (E6 series, Pine Research Instrumentation, USA). Prior to its use, both platinum

ring and glassy carbon disk were polished sequentially with alumina suspensions of 0.5, 0.3, 0.05 µm (Allied Tech Products Inc., USA), followed by sonication with DI water and an electrochemical cleaning procedure in 0.5M H_2SO_4 solution until typical characteristic cyclic voltammograms were obtained.[35, 36] The reference electrode (Ag^+/Ag, RE-7, ALS Co., Ltd) consists of a silver wire, a glass tube filled with a MeCN/0.1 M $TBAClO_4$/0.01 M $AgNO_3$ solution (ALS Co., Ltd) and sealed with a Vycor 7930 frit (ALS Co., Ltd). The reference electrode was assembled in the glovebox at least 24 hours before use and was stored partially immersed in a MeCN/0.1 M $TBAClO_4$ solution. Self-standing $Li_{1-x}FePO_4$ film was used as the counter electrode following a preparation method described elsewhere.[37] The LP30 electrolyte with water content less than 10ppm, as deduced by Karl Fischer titration (Coulometric KF titration, Metrohm), was first purged with argon. The typical volume of electrolyte used was 10mL for each experiment. The potential difference between Ag^+/Ag reference electrode and Li^+/Li redox potential was measured to be 3.19 V in LP30, and all potentials in this work were corrected using this potential difference. All the experiments were operated on an AFMSRCE rotator (PINE Research Instrumentation, USA) and a VMP3 Bipotentiostat (BioLogic Science Instruments, France).

Fabrication of layered oxide disk electrodes.—A blend of active material and carbon super P (Csp) at a 4:1 mass ratio was hand-grinded with N-methyl pyrrolidine (NMP)/poly (vinylidene fluoride) (PVDF) solution for 10 minutes and then stirred for another 1 hour, yielding a slurry with the final concentrations of 10 mg_{oxide} mL_{slurry}^{-1}, 2.5 mg_{Csp} mL_{slurry}^{-1} and 1.25 mg_{PVDF} mL_{slurry}^{-1}. Next, 10 µL of as-prepared slurry was drop-casted onto a 0.196 cm^2 glassy carbon disk. The oxide layer on the glassy carbon disk was dried under vacuum at room temperature for 1 hour prior to be dried further for 6 hours at 55°C under vacuum in

BÜCHI oven. The electrode had a final composition of 100 μg_{oxide}, 25 μg_{Csp}, and 12.5 μg_{pvdf}. The uniformity of such as-prepared electrodes was verified by scanning electron microscopy (SEM) (**Fig. S1**). The Csp electrode was prepared in a similar manner, except that the slurry was obtained with a mixture of Csp and PVDF at a 6:4 mass ratio. The collection efficiency, N, of the RRDE geometry remained unchanged on a Csp supported disk at 25.05% $\pm$ 0.15 as evaluated by the redox reaction of ferrocene/ferrocenium ($K_3Fe(CN)_6$ was not used here due to solubility limitation in LP30 electrolyte) (**Fig. S2**). Similar collection efficiencies were obtained on both bare and Csp-supported disk electrodes which 1) justify the electrode preparation method proposed here and 2) demonstrate that the low collection efficiency found in the present work is originating from gas solubility issues and not from a modification of the laminar flow by the particles.

RRDE measurements.—In order to discern the O_2 gas release phenomenon from Li-rich layered oxides, the oxides of interest deposited on the disk electrode were cycled using linear scan voltammetry, cyclic voltammetry or galvanostatic techniques to extract/insert lithium ions. Additionally, the ring electrode is being held constantly at an oxygen reduction potential, i.e. 2.5V *vs.* Li^+/Li, which was selected based on oxygen reduction measurements performed with a platinum rotating disk electrode (**Fig. S3a**) together with preliminary RRDE measurements which showed that similar O_2 detection potentials were obtained between 2.3 and 2.5V vs. Li^+/Li for $Li_2Ru_{0.5}Ti_{0.5}O_3$ (**Fig. S3b**). So under these conditions, once O_2 is released from the oxide-casted disk electrode and swept outward to the ring electrode by a laminar flow in the bulk electrolyte created by the mechanical rotation of the RRDE tip (ω = 1600 rpm, this rotation rate is sufficient to allow for O_2 removal and limit the bubbles formation from evolved O_2 at the electrode surface), it can be electrochemically detected at

the ring through its reduction ($O_2 + e^- \rightarrow O_2^{\bullet -}$). A schematic representation of the O_2 detection process is presented in **Fig. 1**. Note that all the reported results in this work were at least duplicated two times but not corrected for the background ring current, the magnitude of which being typically less than 3µA. The background ring currents show a tendency to decrease as the residual oxygen and/or impurity in the electrolyte decrease.

***In-situ* pressure analysis.—**Pressure evolutions upon battery operation were monitored by a Swagelok-derived pressure cell[18] which was assembled with metallic lithium counter electrode and two glass fiber separators (Whatman, United Kingdom) soaked with LP30 electrolyte. The active materials were mixed with Csp at a mass ratio of 4:1. After assembly, the cells were kept at open-circuit voltage for at least 10h at a controlled temperature of 25°C in order to stabilize the pressure prior to be cycled.

Online electrochemical mass spectrometry (OEMS).— OEMS measurements were carried out using a homemade OEMS cell. The cell possesses a similar configuration as the pressure cell mentioned above, but with one notable difference: the three-way valve is connected to the inlet capillary of a quadrupole mass spectrometer (Hiden Analytical, HAL 101-RC) via a Swagelok fitting. After assembly in the glove box using metallic lithium counter electrode and two glass fiber separators, the OEMS cell is flushed and pressurized with pure Ar to avoid any contamination from the glove box atmosphere. The cell is then placed in a 25°C climate chamber and connected to the potentiostat and the mass spectrometer (MS). During the OEMS measurements, the internal cell pressure is continuously measured by the pressure sensor and the gaseous species continuously sampled from the cell head space to the mass spectrometer via a thin capillary (1/16" diameter) at a flow rate of 12.5µL min^{-1}.

After ionization in the ionization source of the MS, separation in the mass analyzer and further detection in the ion detector, the partial pressures are eventually determined for each gas based on their mass to charge ratio (m/z). The partial pressures at m/z = 32, m/z = 44 were used to determine the evolution of O_2 and CO_2, respectively. All the partial pressure signals were normalized to the partial pressure of the ^{36}Ar isotope to correct for fluctuations of pressure. The specific gas evolution rate is obtained by processing the first order derivative of the normalized partial pressure vs. time profile. The cell is first typically held at OCV for ~1.5 hours to reach a gas-liquid equilibrium phase inside the cell, and therefore to obtain a stable baseline value for all partial pressure signals. After the OCV period, the galvanostatic charging procedure is started.

Results and discussion

Classical $Li(Ni_xMn_yCo_z)O_2$ denoted NMC which are presently used in commercial Li-ion batteries do not show O_2 release upon oxidation in contrast to the layered Li-rich phases.[8, 15, 38-41] Thus, as a proof of concept to demonstrate the usage of RRDE for oxygen detection we decided to first investigate two NMC phases: the stoichiometric $LiNi_{1/3}Mn_{1/3}Co_{1/3}O_2$ (NMC111) and the Li-rich $Li_{1.2}Ni_{0.13}Mn_{0.54}Co_{0.13}O_2$ (Li-rich NMC) phases. **Figs. 2a** and **2b** present their voltage and internal pressure change profiles as a function of capacity. The cell with Li-rich NMC displays a discernable increase of pressure during the high-voltage charging plateau (from *a* to *b*) followed by a rapid pressure growth (from *b* to the end of charge) (bottom panel in **Fig. 2a**). The two different pressure increments (from *a* to *b*, and from *b* to the end of charge) during the charge period indicate the presence of at least two different

phenomena governing the release of gases, which will be further discussed below. Unlike for Li-rich NMC, only a minor increase of the pressure was measured for NMC111 for the whole charge (from *f*, bottom panel in **Fig.2b**), suggesting negligible gas evolution. In order to discern the chemical nature of the evolved gases, OEMS measurements were further carried out. **Figs. 2c&2d** show the OEMS data obtained with NMC111 and Li-rich NMC during their first charges followed by an OCV step for 0.5h. Starting with the Li-rich NMC (**Fig. 2c**), an evolution of O_2 was measured only after the high-voltage charging plateau (starting from *d*). Unlike for O_2, the CO_2 evolution starts at the beginning of the high-voltage charging plateau (from *c*), before to dramatically increase at the end of charge simultaneously with the evolution of O_2 (from *d*). These results are in good agreement with previous reports.[9] Moreover, they explain the results previously obtained by pressure analysis (**Fig. 2a**) with the initial slight increase of pressure (from *a* to *b*) originating solely from CO_2 evolution, while both O_2 and CO_2 evolution contribute to the second rapid pressure build-up (from *b* to the end of charge). In the case of NMC111 cell (**Fig. 2d**), CO_2 was the only detected gas, accounting for the minor pressure build-up previously observed in pressure cell, while no O_2 evolution was observed during the charge and OCV period.

Knowing that O_2 is evolved at the end of charge for Li-rich NMC but not for NMC111, RRDE measurements were then performed for both materials. The respective voltage-capacity profiles are presented in **Figs. 2e** and **2f** (top panels) and are in agreement with those obtained with pressure and OEMS cells. Turning to the ring current, an increase of the reduction current was measured for Li-rich NMC close to the end of charge (from *e*, **Fig. 2e**), alike the potential at which O_2 was previously detected by OEMS and pressure measurements. In contrast, no such cathodic current increase was observed (bottom panel

in **Fig. 2f**) for NMC111 in agreement with the absence of O_2 release, as deduced from OEMS. The obvious correlation of the reduction current increase with the oxygen evolution for Li-rich NMC, as well as the absence of cathodic current increase and oxygen release for NMC111, allows us to attribute the increase of reduction current to the electrochemical reduction of O_2 evolved from Li-rich NMC. Since the evolution of O_2 is accompanied by the evolution of CO_2, as shown by our OEMS measurement with Li-rich NMC (**Fig. 2c**), the effect of CO_2 generation on the detection of O_2 at the ring electrode was then considered. As previously mentioned, the release of CO_2 begins for Li-rich NMC at an earlier stage of the charge (before the plateau, from *c*, **Fig. 2c**) compared to the onset potential for O_2 generation (after the plateau, from *d*, **Fig. 2c**). However, an increase of reduction current was only recorded at the ring after the plateau (from *e*, **Fig. 2e**) where O_2 starts to release. Therefore, one can conclude that RRDE specifically detects O_2 while being silent to CO_2 when holding the ring potential at 2.5 V vs. Li^+/Li. This conclusion is further supported by performing RRDE measurements with a mixture of NMC111 and Li_2CO_3 (known to evolve CO_2 but not O_2 within the charging potential range)[37, 42] where no modification for the ring current response is observed compared to pure NMC111 (**Figure S4**). Bearing in mind that the ring electrode detects every soluble product that could be reduced/oxidized at the ring potential (impurities, dissolved metal ions from oxides and/or counter electrodes, electrolyte degradation products, etc.), we then evaluate whether species other than O_2 could contribute to the increase of the cathodic ring current upon charging Li-rich NMC. For that, bare and Csp-loaded glassy carbon disk electrodes were measured in cyclic voltammetry mode up to 4.8V vs. Li^+/Li. Doing so, no increase of the reduction current was observed at the ring (**Fig. S5**), and therefore detection of species originating from the carbon additive, binder and/or direct electrolyte oxidation could be excluded. Finally, to

demonstrate the feasibility of the proposed RRDE method for O_2 detection, linear scan voltammetry mode was applied at the disk electrode instead of galvanostatic charging, giving a good agreement between RRDE and pressure cell measurements (**Fig. S6**). Hence, by comparing with *in-situ* pressure and OEMS measurements, we could demonstrate that the RRDE method can selectively detect O_2 generated from Li-rich NMC.

To assess if the RRDE method can be utilized to detect oxygen release for other Li-rich compounds, we further extended our work to the Li_2MO_3 family,[3, 43, 44] with a special attention paid to the $Li_2Ru_{1-y}Ti_yO_3$ series which was previously shown to evolve O_2 at high potentials.[34] Applying the same methodology, we first monitored the gas release upon charging for $Li_2Ru_{0.5}Ti_{0.5}O_3$ with pressure cell (**Fig. 3a**). A slight increase of the internal cell pressure was recorded at the beginning of the high-voltage charging plateau (from *a* to *b*, **Fig. 3a**), followed by a rapid growth (from *b* to the end of charge). Subsequently, OEMS measurements show that the evolution of CO_2 begins at around 4.0V vs. Li^+/Li (line *c*, **Fig. 3b**), which correlates well with the onset of pressure increase detected by pressure cell (line *a*, **Fig. 3a**). Thereafter, O_2 is found to evolve at a relatively higher rate in comparison to the CO_2 evolution (from *d*, **Fig. 3b**). In conclusion, upon charging $Li_2Ru_{0.5}Ti_{0.5}O_3$, CO_2 first evolves, resulting in a small pressure increase before the evolution of O_2 at a higher rate at the end of charge which is associated with the evolution of CO_2 gas, thus leading to a rapid growth of pressure. Now switching to the RRDE technique (**Fig. 3c**), an increase of the cathodic current was recorded at the ring electrode (from *e*, bottom panel), similarly to Li-rich NMC phase. The onset of this ring current increase (~4.0V vs. Li^+/Li) is in good agreement with the onset of O_2 evolution measured by OEMS (~4.06V vs. Li^+/Li), which indicates that O_2 is evolved from $Li_2Ru_{0.5}Ti_{0.5}O_3$ and is detected at the ring via its electrochemical reduction. It is worth

mentioning that the capacity obtained in charge with the RRDE was ~20% smaller compared to those obtained with pressure and OEMS cells. This can be explained by the different cell configurations and the fact that a small portion of the oxide remains inactive due to the lack of stacking pressure in RRDE cell. Unlike for $Li_2Ru_{0.5}Ti_{0.5}O_3$, similar capacities were obtained for NMCs materials by RRDE, pressure and OEMS cells, which suggests a better electronic conductivity when compared to $Li_2Ru_{1-y}Ti_yO_3$ series.

The effect of titanium substitution in $Li_2Ru_{1-y}Ti_yO_3$ series on the O_2 evolution was then studied by measuring $Li_2Ru_{0.75}Ti_{0.25}O_3$. As seen in **Figs. 4a** and **4b**, the evolution of O_2 begins at around 4.1V vs. Li^+/Li (line *d*), leading to a rapid growth in internal cell pressure (from *b* to the end of charge). As expected, an increase of ring reduction current was recorded by RRDE at this potential (from *e*, **Fig. 4c**), indicating the reduction (detection) of O_2. This result clearly confirms that the proposed RRDE method is capable of probing the release of O_2 in various Li-rich materials. Finally, we could demonstrate the reproducibility of these results. For that, two repetitive RRDE experiments were performed with $Li_2Ru_{0.75}Ti_{0.25}O_3$. As seen in **Fig. S7**, nearly identical disk electrochemical performances (showing the charge of the oxide) and ring current responses (corresponding to the detection of O_2) were obtained. In parallel, reproducible tests were also made with $Li_2Ru_{0.5}Ti_{0.5}O_3$ phase (not shown here).

At this stage of the study, the sensitivity of the RRDE technique is worth discussing. As seen in **Fig. S8**, when using the same amount of active material for pressure analysis as for the RRDE study (~100µg), the pressure measured upon charging for $Li_2Ru_{0.75}Ti_{0.25}O_3$ remained nearly constant when using a scan rate of 0.5mV s^{-1} (green curve) or 1.0mV s^{-1} (blue curve). Only when a slower scan rate was applied (0.1mV s^{-1}, red curve), hence

allowing for a longer time for gas accumulation in the headspace and most likely a larger amount of O_2 gas release, a pressure increase was then recorded. In fact, the mass loading of active materials used for pressure analyses and OEMS experiments were respectively ≈70 and 130 times greater than that used for the RRDE measurements. The capability of RRDE method in detecting O_2 at a significant lower mass loading (lower O_2 concentrations) suggests a greater sensitivity. Therefore, the RRDE can be expected to be a useful tool for studying some materials for which a very tiny amount of O_2 is released, which may be below the detection limit of the pressure analysis or OEMS. We should note that all the results reported herein were not normalized to the loading of active materials, therefore the magnitude of pressure build-up, O_2 mass signal and ring currents increment should not be considered for quantitative comparison or sensitivity indicators.

To further evaluate the potential use of RRDE to accurately determine the charging state at which oxygen is released from Li-rich compounds, cyclic voltammetry experiments were carried out for $Li_2Ru_{0.75}Ti_{0.25}O_3$ at various scan rates using both pressure cell and the RRDE set-up. During the RRDE tests, the onset potential for O_2 release was constantly determined at ~4.03V vs. Li^+/Li at every scan rate (**Fig. 5a**), while for pressure measurements the measured onset potentials for gas release vary with the scan rates (**Fig. 5b**). This different behavior is in fact not surprising when considering the different working principles for these two techniques. In pressure measurements, the gaseous species generated at the electrode must first diffuse through the electrolyte and accumulate in the headspace of the electrochemical cell before being detected by the pressure sensor. Unlike for pressure measurements, with the RRDE setup, the transport of species like O_2 is controlled by the convection movement, i.e. the laminar electrolyte flow created by mechanical rotation,

which is faster than the diffusion of species in solutions. Aside from the faster rate for O_2 transport in RRDE set-up, the unique ring-disk geometry also provides a shorter transport length for O_2 than in a pressure cell. Besides, the sensitivity of pressure measurement (and also OEMS) is jeopardized by the amount of gas dissolved into the electrolyte as well as the dead volume of the electrochemical cell, which is not the case for RRDE method where O_2 can be detected once it is generated at the disk and swept outwards the ring electrode. Hence, RRDE is a complementary technique to the pressure measurement and the OEMS which can be employed to accurately determine the onset potential for oxygen release and the effect of charging rate on such gas evolution.

After demonstrating that RRDE can accurately detect the oxygen loss for Li-rich compounds during their initial charges, the electrochemical behavior for $Li_2Ru_{0.5}Ti_{0.5}O_3$ and $Li_2Ru_{0.75}Ti_{0.25}O_3$ compounds during the second voltammetric cycles were recorded (**Fig. S9**). The results reveal a very limited increase of the ring currents arising from the reduction of O_2 generated on the surface of these two compounds, which is consistent with the small irreversibility previously observed during galvanostatic cycling after the first charge.[34]

The question then comes to the quantitative analysis of the amounts of O_2 generated at the disk which can theoretically be deduced from the integration of the cathodic ring current. Comparing the results obtained for $Li_2Ru_{0.5}Ti_{0.5}O_3$ (**Fig. 6a**) and $Li_2Ru_{0.75}Ti_{0.25}O_3$ (**Fig. 6b**), the quantity of O_2 released from $Li_2Ru_{0.5}Ti_{0.5}O_3$ was calculated to be larger than that from $Li_2Ru_{0.75}Ti_{0.25}O_3$ with respectively 1.036% and 0.62% loss of the total oxygen content (for details, see the **Supporting Information**). This trend correlates well with the electrochemical performance for which a greater irreversibility was observed during the first cycle with increased titanium substitution in the $Li_2Ru_{1-x}Ti_xO_3$ series.[34] However, discrepancy arises

when comparing their final compositions after the initial charge calculated based on RRDE and pressure measurements. For $Li_2Ru_{0.5}Ti_{0.5}O_3$, a composition of $Li_{0.65}Ru_{0.5}Ti_{0.5}O_{2.74}$ was obtained from the pressure increase by assuming that all the detected gas is oxygen, whereas a composition of $LiRu_{0.5}Ti_{0.5}O_{2.97}$ is calculated from the RRDE results assuming a collection efficiency of 25% (**Table S1**). Even though the contribution from other gas components such as CO_2 to the pressure evolution has not been taken into account, the expected value for oxygen loss measured by RRDE should be higher since O_2 is the main gas evolved upon charging for $Li_2Ru_{0.5}Ti_{0.5}O_3$, as deduced from OEMS measurements (**Fig. 3b**). Such discrepancy could likely arise from the lower collection efficiency for O_2 at the ring electrode compared to the theoretical value given by the geometrical parameters of the RRDE tip (25.05% $\pm$ 0.15 with the geometry used in this study). Indeed, this theoretical value is only achieved for soluble species such as ferrocene (**Fig. S2**), while for dissolved gas like O_2, limitations related to a limited O_2 solubility in the supporting electrolytes as well as possible bubble formation from the evolved O_2, as discussed elsewhere,[32, 45] can significantly lower the experimental efficiency. Besides, a precise quantification of the amount of oxygen release is further made complex by the fact that small errors in the ring current and the mass loading can lead to a relatively large deviation for the calculated quantity of O_2 release. This is especially true considering the small amounts of active materials used for the RRDE measurements. Therefore, we believe that the amounts of O_2 measured from the ring currents can be used for comparing the quantity of O_2 generation for different phases, but caution must be exercised and the values obtained by RRDE should be complemented by other techniques such as DEMS and/or pressure cells for quantification purposes.

Conclusion

In summary, we have shown that the RRDE method can be employed for monitoring the O_2 release upon charge for Li-rich layered oxides. This simple methodology includes two sequential steps: (1) the deposition of oxides onto the surface of the disk electrode via a simple drop-casting method followed by (2) a standard electrochemical procedure using cyclic voltammetry or galvanostatic cycling to control the delithiation/lithiation processes while the ring electrode is maintained at a potential at which oxygen reduction reaction takes place, allowing for the detection of O_2 released from the oxides. To validate the proposed methodology, RRDE measurements were first carried out with various Li-rich layered oxides. The obtained results were further compared with those obtained by OEMS and pressure cell. In doing so, we could demonstrate that RRDE 1) selectively detect oxygen while being silent to other species potentially generated at high potentials, 2) shows better sensitivity and reliability than the aforementioned techniques which allows for the detection of O_2 at relatively lower concentrations, 3) enable a precise determination of the O_2 release potential, and 4) can be used for a fast-screening of the O_2 release phenomena in a wide variety of new materials owing to the wide-spread of such techniques in the fields of batteries or electrocatalysis. Additionally, its reproducibility was demonstrated using repetitive tests. Nevertheless, caution must be exercised when tentatively quantifying the amount of O_2 generated during the charging process at the disk. Overall, the RRDE method comes as a valuable complement to the already existing gas pressure/gas analysis techniques such as OEMS and pressure cell which usually do not allow from either quickly screening multiple materials for OEMS or for specifically detecting O_2 for the pressure

measurements. In principle, one can expect this method to be extended to the detection of other gases such as CO_2 or soluble species. For that, the selection of the adequate ring electrode will be crucial since it should selectively reduce or oxidize the gas or species of interest (Copper ring for CO_2 for instance) without jeopardizing the electrochemical/chemical stability of the whole system.

Figures:

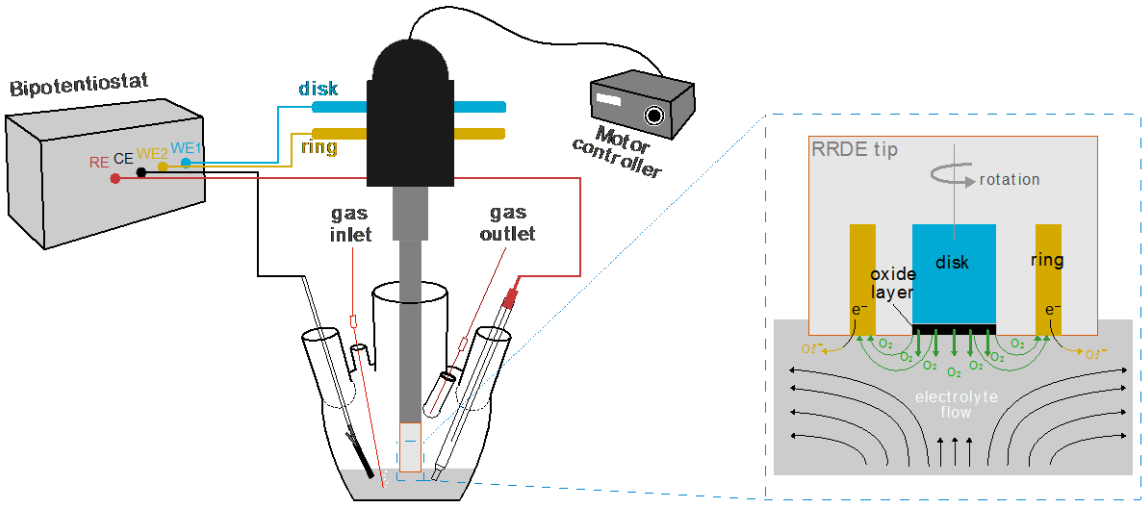

Figure 1. Schematic illustration of the RRDE system and the four-electrode cell configuration (left side), WE1, WE2, CE and RE stand for working electrode 1 (disk electrode), working electrode 2 (ring electrode), counter electrode and reference electrode, respectively. A magnified view of the RRDE tip and its near-electrolyte region depicts the transport and redox processes occurring in the RRDE system designed to assess the O_2 release phenomenon in Li-rich layered oxides (right side).

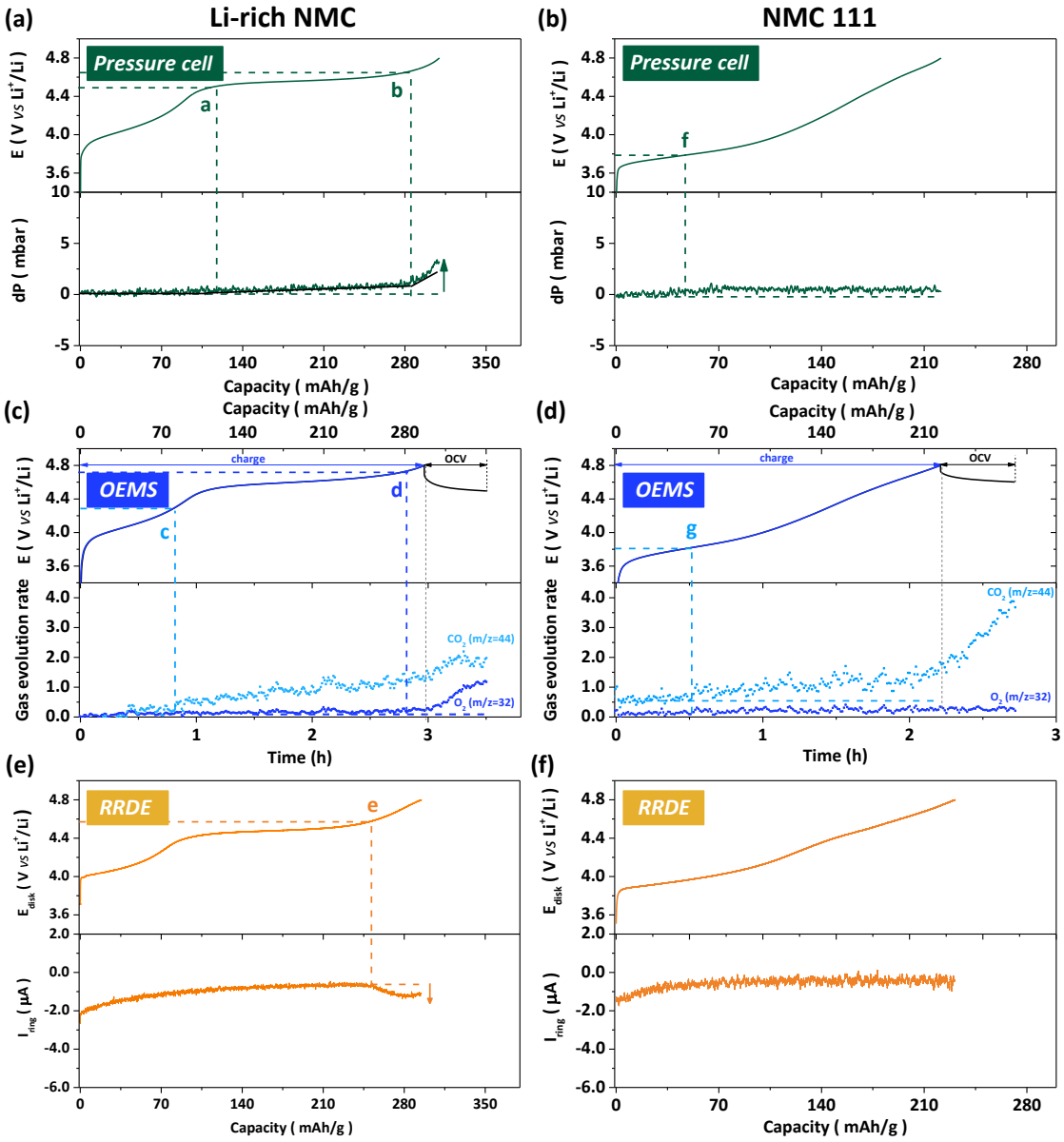

Figure 2. Galvanostatic charge curves (top panels) and their respective pressure change (bottom panels) for Li-rich NMC (a) and NMC111 (b) in pressure cells. Potential (top panels) and gas evolution rate (bottom panels) as a function of time (and capacity) for Li-rich NMC (c) and NMC111 (d) measured by OEMS. RRDE profiles measured for Li-rich NMC (e) and NMC111 (f) in LP30 electrolytes. Top panels present the galvanostatic charge curves obtained in the disk. Bottom panels illustrate their corresponding ring current response. All the cells are charged at a current rate of 0.3C to 4.8V *vs.* Li^+/Li. Gas evolution onsets are defined by dash lines labeled from *a* to *g* as guide for the eye.

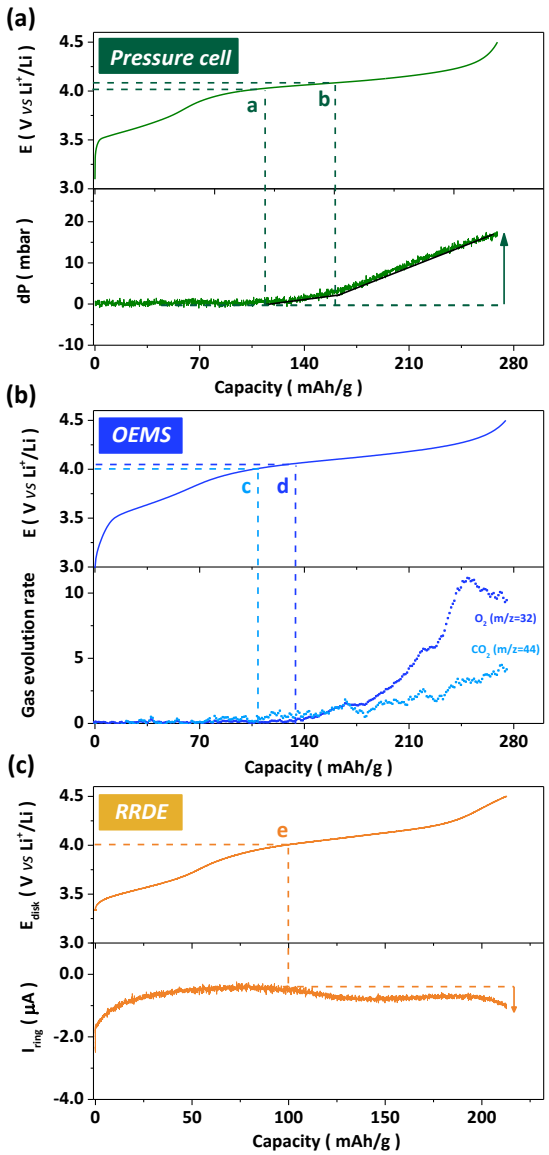

Figure 3. (a) Galvanostatic charge curve (top panel) and its respective pressure change (bottom panel) for $Li_2Ru_{0.5}Ti_{0.5}O_3$ in pressure cell. (b) Potential (top panel) and gas evolution rate (bottom panel) as a function of capacity for $Li_2Ru_{0.5}Ti_{0.5}O_3$ measured by OEMS. (c) RRDE profiles for $Li_2Ru_{0.5}Ti_{0.5}O_3$ measured in LP30 electrolytes. Top panel shows the galvanostatic charge curve obtained in the disk. Bottom panel illustrates its corresponding ring current response. All the cells are charged at a current rate of 0.3C to 4.5V *vs.* Li^+/Li. Gas evolution onsets are defined by dash lines labeled from *a* to *e* as guide for the eye.

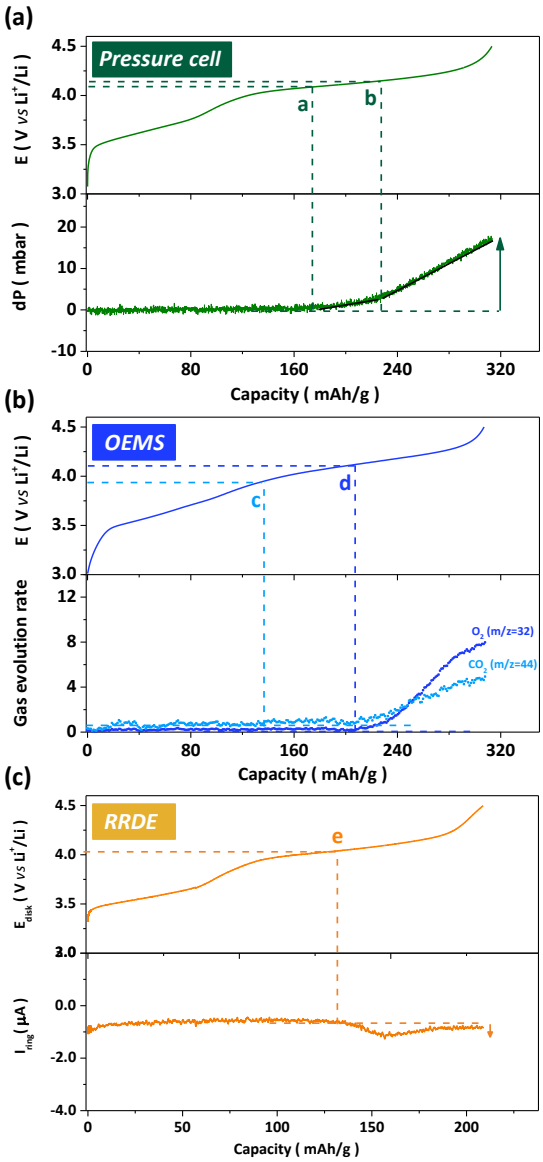

Figure 4. (a) Galvanostatic charge curve (top panel) and its respective pressure change (bottom panel) for $Li_2Ru_{0.75}Ti_{0.25}O_3$ in pressure cell. (b) Potential (top panel) and gas evolution rate (bottom panel) as a function of capacity for $Li_2Ru_{0.75}Ti_{0.25}O_3$ measured by OEMS. (c) RRDE profiles for $Li_2Ru_{0.75}Ti_{0.25}O_3$ measured in LP30 electrolytes. Top panel shows the galvanostatic charge curve obtained in the disk electrode. Bottom panel illustrates its corresponding ring current response. All the cells are charged at a current rate of 0.3C to 4.5V *vs.* Li^+/Li. Gas evolution onsets are defined by dash lines labeled from *a* to *e* as guide for the eye.

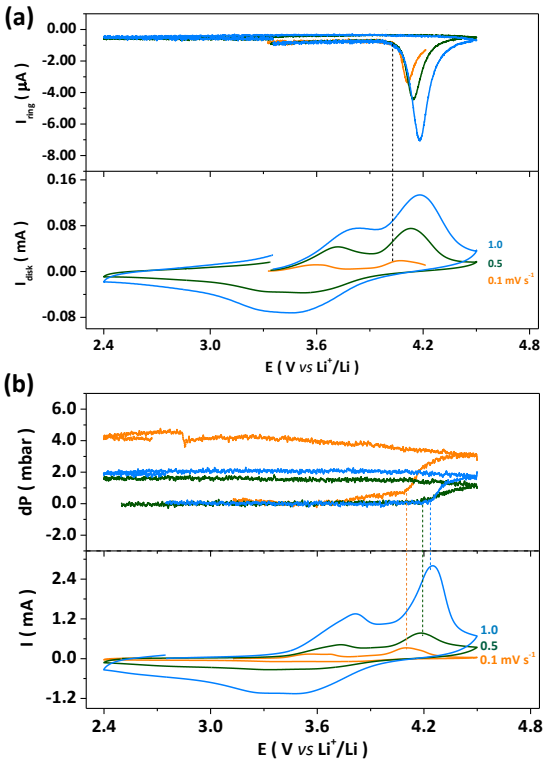

Figure 5 Comparison of RRDE profiles (a) and *in-situ* pressure analysis (b) for $Li_2Ru_{0.75}Ti_{0.25}O_3$ recorded at various scan rates: 0.1mV s^{-1} (yellow line), 0.5mV s^{-1} (green line), and 1.0mV s^{-1} (blue line). The cyclic voltammograms are presented in the bottom panels and their respective ring current response (a), and pressure change (b) are shown in the top panels.

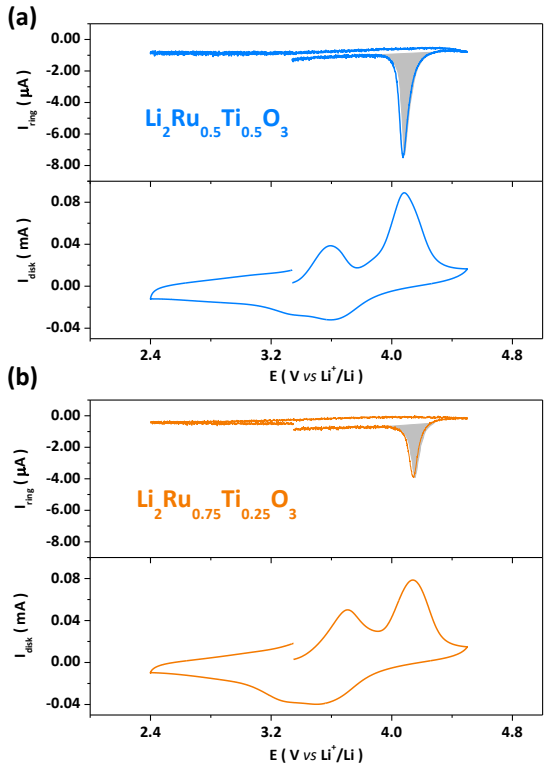

Figure 6. Comparison of RRDE profiles for $Li_2Ru_{0.5}Ti_{0.5}O_3$ (a) $Li_2Ru_{0.75}Ti_{0.25}O_3$ (b) recorded at a scan rate of 0.5mV s^{-1} with the cyclic voltammograms presented in the bottom panels and their respective ring current evolution shown in the top panels. The grey shaded area in the top panels represents the increment of cathodic ring current due to the reduction of detected O_2.

ACKNOWLEDGMENTS

The authors would like to thank P. Lemaire for some electrodes preparation and D. Alves Dalla Corte for the SEM images. A.G. and J.-M.T. would like to acknowledge funding from the European Research Council (ERC) (FP:2014)/ERC Grant-Project 670116-ARPEMA. W.YIN acknowledges a fellowship from the China Scholarship Council (CSC) to perform this work at UPMC and Collège de France.

Supporting Information Available: Supporting information include Figures S1-S9, calculation method of the amount of O_2 release and Table S1.

Reference:

1. **N. Yabuuchi, K. Yoshii, S. T. Myung, I. Nakai, and S. Komaba, *J. Am. Chem. Soc,* 133 4404-4419 (2011).**
2. **H. Koga, L. Croguennec, M. Menetrier, K. Douhil, S. Belin, L. Bourgeois, E. Suard, F. Weill, and C. Delmas, *J. Electrochem. Soc,* 160 A786-A792 (2013).**
3. **M. Sathiya, G. Rousse, K. Ramesha, C. P. Laisa, H. Vezin, M. T. Sougrati, M.-L. Doublet, D. Foix, D. Gonbeau, W.Walker, A. S. Prakash, M. B. Hassine, L. Dupont, and J.-M. Tarascon, *Nat. Mater,* 12 827-835 (2013).**
4. **J. Choi and A. Manthiram, *J. Electrochem. Soc,* 152 A1714-A1718 (2005).**
5. **V. Pimenta, M. Sathiya, D. Batuk, A. M. Abakumov, D. Giaume, S. Cassaignon, D. Larcher, and J.-M. Tarascon, *Chem. Mater.,* 29 9923-9936 (2017).**
6. **P. Rozier and J. M. Tarascon, *J. Electrochem. Soc,* 162 A2490-A2499 (2015).**
7. **G. Assat and J.-M. Tarascon, *Nat. Energy,* 3 373-386 (2018).**
8. **A. R. Armstrong, M. Holzapfel, P. Novak, C. S. Johnson, S.-H. Kang, M. M. Thackeray, and P. G. Bruce, *J. Am. Chem. Soc,* 128 8694-8698 (2006).**
9. **B. Strehle, K. Kleiner, R. Jung, F. Chesneau, M. Mendez, H. A. Gasteiger, and M. Piana, *J. Electrochem. Soc,* 164 A400-A406 (2017).**
10. **A. J. Perez, Q. Jacquet, D. Batuk, A. Iadecola, M. Saubanère, G. Rousse, D. Larcher, H. Vezin, M.-L. Doublet, and J.-M. Tarascon, *Nat. Energy,* 2 954-962 (2017).**
11. **E. McCalla, A. M. Abakumov, M. Saubanère, D. Foix, E. J. Berg, G. Rousse, M.-L. Doublet, D. Gonbeau, P. Novák, G. V. Tendeloo, R. Dominko, and J.-M. Tarascon, *Science,* 350 1516-1521 (2015).**
12. **Y. Xie, M. Saubanère, and M. L. Doublet, *Energy Environ. Sci.,* 10 266-274 (2017).**
13. **M. Saubanère, E. McCalla, J. M. Tarascon, and M. L. Doublet, *Energy Environ. Sci.,* 9 984-991 (2016).**
14. **D.-H. Seo, A. Urban, and G. Ceder, *Nat.Chem.,* 8 692-697 (2016).**
15. **F. La Mantia, F. Rosciano, N. Tran, and P. Novák, *J. Electrochem. Soc,* 156 A823-A827 (2009).**

16. J. Uddin, V. S. Bryantsev, V. Giordani, W. Walker, G. V. Chase, and D. Addison, *J. Phys. Chem. Lett,* 4 3760-3765 (2013).
17. V. Giordani, D. Tozier, H. Tan, C. M. Burke, B. M. Gallant, J. Uddin, J. R. Greer, B. D. McCloskey, G. V. Chase, and D. Addison, *J. Am. Chem. Soc.,* 138 2656-2663 (2016).
18. F. Lepoivre, A. Grimaud, D. Larcher, and J. M. Tarascon, *J. Electrochem. Soc.,* 163 A923-A929 (2016).
19. W. J. Albery and J. S. Drur, *Trans. Faraday Soc.,* 62 1915-1919 (1966).
20. F. Dalton, *Electrochem. Soc. Interface,* 25 50-59 (2016).
21. Y. Wang, N.-C. Lai, Y.-R. Lu, Y. Zhou, C.-L. Dong, and Y.-C. Lu, *Joule,* (2018).
22. W. Wang, N. C. Lai, Z. Liang, Y. Wang, and Y. C. Lu, *Angew. Chem. Int. Ed.,* 5042-5046 (2018).
23. R. J. Behm, U. A. Paulus, T. J. Schmidt, and H. A. Gasteiger, *J. Electroanal. Chem,* 495 134–145 (2001).
24. F. d. r. Jaouen and J.-P. Dodelet, *J. Phys. Chem. C,* 113 15422-15432 (2009).
25. J. Herranz, A. Garsuch, and H. A. Gasteiger, *J. Phys. Chem. C,* 116 19084-19094 (2012).
26. C. Xia, R. Black, R. Fernandes, B. Adams, and L. F. Nazar, *Nat. Chem.,* 7 496-501 (2015).
27. S. Sankarasubramanian, J. Seo, F. Mizuno, N. Singh, and J. Prakash, *J. Phys. Chem. C,* 121 4789-4798 (2017).
28. Y.-C. Lu, Q. He, and H. A. Gasteiger, *J. Phys. Chem. C,* 118 5733-5741 (2014).
29. L.-F. Wang, C.-C. Ou, K. A. Striebel, and J.-S. Chen, *J. Electrochem. Soc,* 150 A905-A911 (2003).
30. R. G. Buchheit, M. A. Martinez, and L. P. Montes, *J. Electrochem. Soc,* 147 119-124 (2000).
31. J. Li, W. Sun, B. Hurley, A. A. Luo, and R. G. Buchheit, *Corros. Sci,* 112 760-764 (2016).
32. C. C. McCrory, S. Jung, J. C. Peters, and T. F. Jaramillo, *J. Am. Chem. Soc,* 135 16977-16987 (2013).
33. J. Scholz, M. Risch, K. A. Stoerzinger, G. Wartner, Y. Shao-Horn, and C. Jooss, *J. Phys. Chem. C,* 120 27746-27756 (2016).
34. M. Sathiya, A. M. Abakumov, D. Foix, G. Rousse, K. Ramesha, M. Saubanère, M. L. Doublet, H. Vezin, C. P. Laisa, A. S. Prakash, D. Gonbeau, G. VanTendeloo, and J.-M. Tarascon, *Nat. Mater,* 14 230-238 (2014).
35. N. M. MarkoviC, H. A. Gasteiger, and J. Philip N. Ross, *J Phys Chem.,* 99 3411-3415 (1995).
36. J. Solla-Gullo´n, V. Montiel, A. Aldaz, and J. Clavilier, *J. Electroanal. Chem,* 491 69-77 (2000).
37. W. Yin, A. Grimaud, F. Lepoivre, C. Yang, and J.-M. Tarascon, *J. Phys. Chem. Lett.,* 8 214–222 (2017).
38. F. La Mantia, F. Rosciano, N. Tran, and P. Novák, *J Appl Electrochem.,* 38 893-896 (2008).
39. A. Guéguen, D. Streich, M. He, M. Mendez, F. F. Chesneau, P. Novák, and E. J. Berg, *J. Electrochem. Soc,* 163 A1095-A1100 (2016).
40. K. Luo, M. R. Roberts, K. Edström, J. Guo, RongHao, N. Guerrini, A. V. Chadwick, D. M. Pickup, L. C. Duda, P. G. Bruce, and Y.-S. Liu, *Nat. Chem.,* 8 684-691 (2016).
41. R. Jung, M. Metzger, F. Maglia, C. Stinner, and H. A. Gasteiger, *J. Electrochem. Soc,* 164 A1361-A1377 (2017).
42. S. Yang, P. He, and H. Zhou, *Energy Environ. Sci.,* 9 1650-1654 (2016).
43. H. Chen and M. S. Islam, *Chem. Mater.,* 28 6656-6663 (2016).
44. B. Li, R. Shao, H. Yan, L. An, B. Zhang, H. Wei, J. Ma, D. Xia, and X. Han, *Adv. Funct. Mater,* 26 1330-1337 (2016).
45. Q. Gao, C. Ranjan, Z. Pavlovic, R. Blume, and R. Schlögl, *ACS Catal.,* 5 7265-7275 (2015).